

**Collisional dynamics of ultracold OH molecules in an electrostatic field**

Alexandr V. Avdeenkov and John L. Bohn

*JILA and Department of Physics, University of Colorado, Boulder, Colorado 80309*

(Received 29 March 2002; published 22 November 2002)

Ultracold collisions of polar OH molecules are considered in the presence of an electrostatic field. The field exerts a strong influence on both elastic and state-changing inelastic collision rate constants, leading to clear experimental signatures that should help disentangle the theory of cold molecule collisions. Based on the collision rates, we discuss the prospects for evaporative cooling of electrostatically trapped OH. We also find that the scattering properties at ultralow temperatures prove to be remarkably independent of the details of the short-range interaction, owing to avoided crossings in the long-range adiabatic potential curves. The behavior of the scattering rate constants is qualitatively understood in terms of a novel set of long-range states of the  $[\text{OH}]_2$  dimer.

DOI: 10.1103/PhysRevA.66.052718

PACS number(s): 34.20.Cf, 34.50.-s, 05.30.Fk

**I. INTRODUCTION**

Polar molecules bring something entirely new to the field of ultracold physics. As compared to the neutral atoms that have been studied experimentally in the past, polar molecules possess extremely strong, anisotropic interactions. It has been speculated that dipolar interactions will lead to new properties in Bose-Einstein condensates [1–3] or degenerate Fermi gases [4]. It has also been suggested that polar molecules in optical lattices may be useful in implementing quantum logic elements [5]. On the experimental side, cold polar molecules may be produced in several ways, including photoassociation of two distinct alkali species [6,7], buffer-gas cooling [8,9], or Stark slowing [10–12].

Regardless of the method of production, collisions of molecules are of paramount importance in describing the properties of the gas. Collisions should also be interesting in their own right, as detailed probes of intermolecular interactions. Several features of the collisional dynamics of ground-state polar molecules, based on a simplified “toy” model, were discussed in Ref. [13]. This model accounted for the interplay between the dipole-dipole interactions, an external electric field, and the states of different parities. The dipole-dipole interaction, which scales with intermolecular separation  $R$  as  $1/R^3$ , renders cold molecule collisions completely different from cold atom collisions. This is because a pure  $1/R^3$  interaction is characterized by energy-independent low-energy cross sections in *all* partial waves  $l > 0$ , and logarithmically divergent cross sections for  $l = 0$  [14–16]. The relatively strong, long-range interactions imply that molecules electrostatically trapped in weak-field-seeking states are generally susceptible to state-changing collisions that can rapidly deplete the trapped gas. The rates are, in general, far larger than those of magnetic dipolar transitions in stretched-state alkali atoms, owing largely to the relative strength of electric, as opposed to magnetic, dipolar interactions [13].

In this paper, we address ultracold polar molecule collisions in a more realistic model, considering in detail the OH radical. This choice is motivated by the attractiveness of this molecule for Stark slowing from a supersonic jet [12,17]. In particular, it has a  $^2\Pi$  ground state with a small  $\Lambda$ -doublet splitting, making it easily manipulated by modest-sized elec-

tric fields. A full treatment of cold collisions is somewhat hindered by the fact that the OH-OH potential-energy surface (PES) is poorly known, although it is known to be very deep and strongly anisotropic [19,20]. In recent years, several theoretical methods have been developed to treat molecule-molecule collisions of dipolar molecules at low temperatures, focusing on their long-range electrostatic interaction (for example, see Refs. [21,22] and references therein). Here we focus on the additional subtlety introduced by the addition of an electrostatic field, and its effects on the state-to-state rate constants. It is also not known whether OH molecules may suffer chemical reactions at ultralow temperatures. As a point of reference, it was recently suggested that the reaction  $\text{F} + \text{H}_2 \rightarrow \text{HF} + \text{H}$  may proceed at appreciable rates at ultralow temperatures, in spite of having a chemical barrier height of 700 K [23]. (In this paper, we work in energy units of Kelvin. These are comparable to the more familiar wave-number units of molecular physics, the conversion factor being  $1 \text{ K} = 0.695 \text{ cm}^{-1}$ .)

However, long-range dipole-dipole forces strongly dominate the scattering of OH molecules in their weak-field-seeking states. In this paper, we will show that this arises from strong avoided crossings in the long-range adiabatic potential curves, which prevent the molecules from approaching close enough to one another for exchange potentials to become important. In this regard, cooling and electrostatic trapping of OH molecules can provide a wealth of information on the long-range OH-OH interaction. Thus it appears possible to understand a class of ultracold OH-OH collisions without detailed knowledge of the short-range PES. This strategy would be an important stepping stone toward understanding the full problem of ultracold OH collisions. Strong-field seekers, by contrast, will in addition experience the short-range interaction. The complete problem of exploring collisions of ultracold polar molecules might therefore most efficiently proceed by a two-step analysis, thus simplifying this very complicated problem.

Accordingly, we focus in this paper on the first step, namely, collisions of weak-field-seeking states. After some discussion on the relevant properties of OH molecules in Sec. II and their interactions in Sec. III, we move on in Sec. IV to illustrate some prominent energy- and field-dependent

features in elastic and inelastic cross sections. Mapping these features in experiments should help in unraveling the long-range part of this puzzle. We also present a simplified model of the long-range interaction to help illustrate the basic physics behind the behavior of the cross sections. It will turn out that a new class of long-range bound states of the  $[\text{OH}]_2$  dimer plays a significant role in ultracold collisions of this molecule.

## II. OH MOLECULE

The OH molecule has a fairly complicated internal structure incorporating rotation, parity, electronic spin, and nuclear spin degrees of freedom, which are further confounded in the presence of an electric field. We therefore begin by describing the structure of this molecule, and the simplifications we impose to render our model tractable.

The molecules cooled to subkelvin temperatures by Stark slowing will be assumed to be in their electronic  $^2\Pi$  ground state, and  $\nu=0$  vibrational ground state. In this state, OH is an almost pure Hund's case- $a$  molecule, and has a dipole moment of 1.68 D [19]. Spin-orbit coupling involving the lone electronic spin splitting of the ground state into  $^2\Pi_{3/2}$  and  $^2\Pi_{1/2}$  components, of which  $^2\Pi_{3/2}$  is lower in energy and is therefore the state of greatest interest in ultracold collisions. In our model, we take into account just the lowest rotational level of the corresponding ground state,  $J=3/2$ . The energy of the first rotationally excited state with  $|J=5/2, \Omega=3/2\rangle$  is about 84 K higher in energy [18], and we will neglect this and higher-lying states in our scattering calculations. Such states will, however, contribute rotational Feshbach resonances in realistic collisions.

The isotopomer  $^{16}\text{O}^1\text{H}$  that we consider here has a nuclear spin of  $I=1/2$ , which with a half-integer rotational quantum number defines the OH molecule as a boson. Thus we should take into account the hyperfine structure to ensure the proper Bose symmetry. We will see below that the inclusion of hyperfine structure is also important in determining details of collision properties. The calculations in an electric field also require knowing the Stark splitting for OH molecules. Thus the Hamiltonian for the OH molecule in a field is

$$H^{OH} = H_{rot} + H_{fs} + H_{hfs} + H_{field}. \quad (1)$$

The wave functions for the spatial degrees of freedom of the molecule are constructed in the usual way. Namely, in the zero-electric-field limit, eigenstates of parity  $\varepsilon$  ( $=\pm$ ) are given by the Hund's case- $a$  representation:

$$|JM_J\Omega\varepsilon\rangle = \frac{1}{\sqrt{2}}(|JM_J\Omega\rangle|\Lambda\Sigma\rangle + \varepsilon|JM_J-\Omega\rangle|-\Lambda-\Sigma\rangle), \quad (2)$$

where the rotational part is given by a Wigner function

$$|JM_J\Omega\rangle = \left(\frac{2J+1}{8\pi^2}\right)^{1/2} D_{M_J\Omega}^J(\theta, \phi, \kappa), \quad (3)$$

and  $\Omega = |\Sigma + \Lambda|$  is the projection of the total electronic angular momentum on the molecular axis. The total spin of the molecule,  $\mathbf{F} = \mathbf{J} + \mathbf{I}$ , with laboratory projection  $M_F$ , is then constructed by

$$\begin{aligned} |(JI)FM_F\Omega\varepsilon\rangle &= |\Lambda\rangle|S\Sigma\rangle \\ &\times \sum_{M_J, M_I} |JM_J\Omega\varepsilon\rangle|IM_I\rangle\langle FM_F|JM_JI_{M_I}\rangle. \end{aligned} \quad (4)$$

The matrix elements for the Hamiltonian (1) in this basis can be found elsewhere [25]. In compact form these matrix elements are

$$\begin{aligned} \langle (JI)F\Omega M_F \varepsilon | H^{OH} | (J'I')F'\Omega'M'_F\varepsilon' \rangle &= [\delta_{\Omega,3/2}\delta_{\Omega',3/2}E_{3/2,3/2} + \delta_{\Omega,1/2}\delta_{\Omega',1/2}E_{1/2,1/2} \\ &+ (\delta_{\Omega,3/2}\delta_{\Omega',1/2} + \delta_{\Omega,1/2}\delta_{\Omega',3/2})E_{3/2,1/2}] \\ &\times \delta_{J,J'}\delta_{F,F'}\delta_{\varepsilon,\varepsilon'} - \mu\mathcal{E}\frac{1}{2}[1 + (-1)^{J+J'}\varepsilon\varepsilon'] \\ &(-1)^{F+F'+M_F+I-\Omega+1} \times ([J][J']][F] \\ &\times [F']^{1/2} \begin{pmatrix} J & 1 & J' \\ -\Omega & 0 & \Omega' \end{pmatrix} \begin{pmatrix} F' & 1 & F \\ -M'_F & 0 & M_F \end{pmatrix} \\ &\times \begin{pmatrix} 1 & J & J' \\ I & F & F' \end{pmatrix}. \end{aligned} \quad (5)$$

In this expression  $\mu$  is the molecular dipole moment,  $\mathcal{E}$  is the strength of the electric field, and  $E_{\Omega,\Omega'}$  are matrix elements for the fine structure  $H_{rot} + H_{fs}$ , which can be found in Refs. [25,26]. These values depend on the rotational constant, spin-orbit coupling constant, hyperfine coupling constant, and  $\Lambda$ -doublet parameters of OH. All of these constants can be found in Ref. [18].

Equation (5) shows that  $\Omega$  is not a conserved quantity. However, in view of the fact that OH is nearly a purely Hund's case- $a$  molecule, the coupling between  $\Omega=1/2$  and  $\Omega=3/2$  states is fairly weak. We account for this interaction perturbatively, by replacing the values  $E_{3/2}$  and  $E_{1/2}$  by the eigenvalues of the  $2 \times 2$  matrix

$$\begin{pmatrix} E_{3/2} & E_{3/2,1/2} \\ E_{3/2,1/2} & E_{1/2} \end{pmatrix}, \quad (6)$$

keeping all other quantum numbers constant.

Likewise, different values of the molecular spin  $J$  are mixed in a field, but this mixing is small in laboratory strength fields. The total spin  $F$  and the parity are far more strongly mixed. Accordingly, in practice we transform the molecular state to a field-dressed basis for performing scattering calculations:

$$|(\tilde{J}I)\tilde{F}M_F\tilde{\Omega}\tilde{\varepsilon}; \mathcal{E}\rangle \equiv \sum_{JF\varepsilon} \alpha(JF\varepsilon) |(JI)FM_F\Omega\varepsilon\rangle, \quad (7)$$

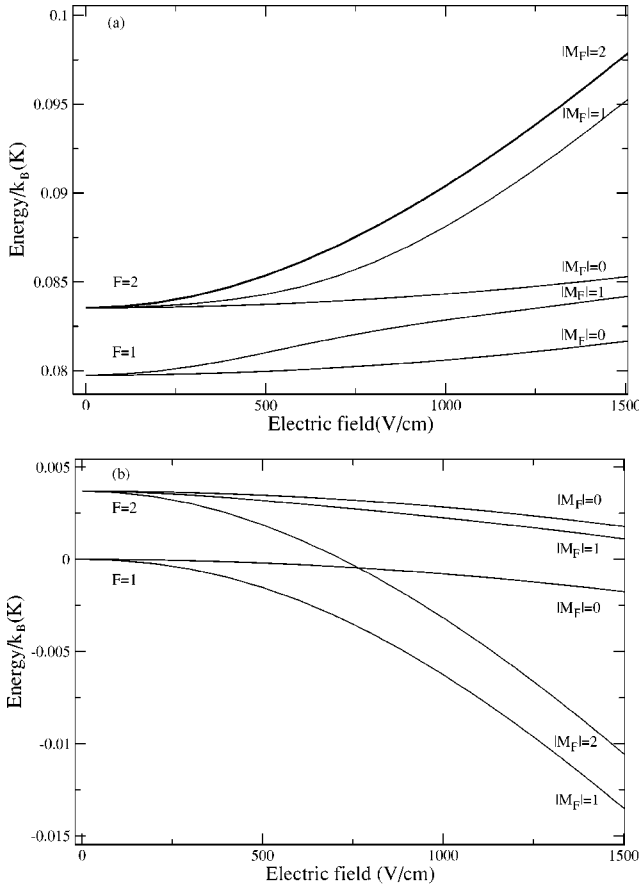


FIG. 1. The Stark effect in ground-state OH molecules, taking into account hyperfine splitting. (a) shows the states that have odd parity  $\varepsilon = -$  in zero electric field ( $f$  states), whereas (b) shows those of even parity ( $e$  states). The weak-field-seeking state with quantum numbers  $F = M_F = 2$ , the subject of this paper, is indicated by the heavy solid line. Note that states with  $M_F = \pm |M_F|$  are degenerate in an electric field.

where  $\alpha(JF\varepsilon)$  stands for eigenfunctions of the Hamiltonian (1) determined numerically at each value of the field. We will continue to refer to the molecular states by the quantum numbers  $J$ ,  $F$ , and  $\varepsilon$ , with the understanding that they are only approximately good in a field, and that Eq. (7) is the appropriate molecular state. Note that the projection  $M_F$  of the total angular momentum on the field axis is a good quantum number.

Figure 1 shows the Stark energies computed using all the ingredients described above. In zero field, the energy levels are primarily determined by the  $\Lambda$ -doublet splitting between opposite parity states, whose value is  $\Delta = 0.0797$  K. The alternative parity states, with  $\varepsilon = -1$  ( $f$  states) and  $\varepsilon = +1$  ( $e$  states) are shown in Figs. 1(a) and 1(b), respectively. These states are further split into hyperfine components with total spin  $F = 1$  and  $F = 2$ . The Stark shift is quadratic for fields below the critical field  $\mathcal{E}_0 \equiv \Delta/2\mu$  ( $\approx 1000$  V/cm for OH). For fields larger than  $\mathcal{E}_0$  states with different parity are entirely mixed and the Stark effect transforms from quadratic to linear. In this case, the molecular states are roughly equal linear combinations of the zero field  $\varepsilon = -$  and  $\varepsilon = +$  states [compare Eq. (2)] [27]:

$$|JM_J\Omega\varepsilon = \pm 1\rangle = \begin{cases} |JM_J\mp\Omega\rangle, & M_J < 0 \\ |JM_J\pm\Omega\rangle, & M_J > 0 \end{cases}. \quad (8)$$

### III. OH-OH INTERACTION

We will consider diatom-diatom scattering as two interacting rigid rotors in their ground rotational states. The complete Hamiltonian for the collision process can then be written as

$$H = T_1 + T_2 + H_1^{OH} + H_2^{OH} + V_s + V_{\mu\mu} + V_{qq} + V_{disp}, \quad (9)$$

where  $T_i$  and  $H_i^{OH}$  are the translational kinetic energy and internal motion of molecule  $i$ , including the electric field as in Eq. (1).  $V_s$  is the short-range exchange interaction,  $V_{\mu\mu} + V_{qq} + V_{disp}$  are the dipole-dipole, quadrupole-quadrupole, and dispersion long-range interactions, respectively. Explicit expression for the dipole-dipole ( $\propto 1/R^3$ ) and quadrupole-quadrupole ( $\propto 1/R^5$ ) interactions are given in Ref. [28]. Matrix elements for the dipole-quadrupole interaction vanish for rigid rotor molecules in identical states [19], hence will not be considered here.

The anisotropic potential between the two interacting rigid-rotor molecules is conveniently recast into a standard set of angular functions [28]:

$$V_s + V_{\mu\mu} + V_{qq} + V_{disp} \equiv V(\omega_A, \omega_B, \omega, R) = \sum_{\Lambda} V_{\Lambda} A_{\Lambda}(\omega_A, \omega_B, \omega), \quad (10)$$

where  $\Lambda \equiv (L_A, K_A, L_B, K_B, L)$  and the angular functions are defined as

$$A_{\Lambda}(\omega_A, \omega_B, \omega) = \sum_{M_A, M_B, M} \begin{pmatrix} L_A & L_B & L \\ M_A & M_B & M \end{pmatrix} \times D_{M_A, K_A}^{L_A}(\omega_A) D_{M_B, K_B}^{L_B}(\omega_B) C_M^L(\omega), \quad (11)$$

where  $\omega_{A,B} = (\theta_{A,B}, \phi_{A,B})$  are the polar angles of molecules  $A$  and  $B$  with respect to the laboratory-fixed quantization axis, and  $\mathbf{R} = (R, \omega)$  is the vector between the center of mass of the molecules in the laboratory-fixed coordinate frame. The indices  $K_A$  and  $K_B$  denote the dependence of the interaction on the orientation of the molecules about their own axes; in what follows we will ignore this dependence, setting  $K_A = K_B = 0$ . For the long-range part of the interaction this approximates the quadrupole moment of OH as cylindrically symmetric.

The exchange potential  $V_s$  is very complicated, consisting of four singlet and four triplet surfaces [20], and is moreover poorly characterized. The most complete treatment of this surface to date computes the lowest-energy potential for each value of internuclear separation  $R$  [19]. This potential finds an extremely deep minimum at  $R = 2.7$  a.u. corresponding to the chemically bound hydrogen peroxide, and a second shallower minimum at  $R = 6$  a.u. due to hydrogen-bonding forces. However, in cold collisions, the scattering cross sec-

tions are so sensitive to details of the short-range interaction that knowing the complete interaction probably would not help anyway. More importantly, as we will see below, collisions of the weak-field-seeking states are strongly dominated by the long-range dipole-dipole interaction. Therefore, we will use at small  $R$  simply the hydrogen-bonding part of the potential surface (see Fig. 13 of Ref. [19]), and we will treat this part of the interaction as if it were isotropic. Finally, we will assert that the spin states of the OH molecules are initially in their stretched states, so that ordinary spin-exchange processes will not play a role in these collisions.

We express the Hamiltonian in a basis of projection of the total angular momentum,

$$\mathcal{M} = M_{F_1} + M_{F_2} + M_{I_1}, \quad (12)$$

$$M_{F_i} = M_{J_i} + M_{I_i}, \quad (13)$$

where  $M_{F_i}$ ,  $M_{J_i}$ , and  $M_{I_i}$  are the projections of the full molecule spin, rotational motion, and nuclear spin on the laboratory axis, respectively, for each molecule.  $M_I$  is the projection of the partial-wave quantum number on the laboratory axis. In this basis the wave function for two molecules is described as

$$\Psi^{\mathcal{M}} = \sum_{1,2,I,M_I} \{|1\rangle \otimes |2\rangle \otimes |IM_I\rangle\}^{\mathcal{M}} \psi^{\mathcal{M},1,2}(R), \quad (14)$$

where  $\{\dots\}^{\mathcal{M}}$  is the angular-momentum part, where  $|i\rangle$  is the wave function for each molecule as described by Eq. (4), and  $\psi^{\mathcal{M},1,2}(R)$  is radial part of this wave function.

Because the target and the projectile are identical bosons, we must take into account the symmetry of the wave function under exchange. The properly symmetrized wave function is then

$$\begin{aligned} & \{|1\rangle \otimes |2\rangle \otimes |IM_I\rangle\}^s \\ &= \frac{\{|1\rangle \otimes |2\rangle \otimes |IM_I\rangle\} + (-1)^I \{|2\rangle \otimes |1\rangle \otimes |IM_I\rangle\}}{\sqrt{2(1 + \delta_{12})}}. \end{aligned} \quad (15)$$

Using the expansion of the intermolecular potential (10), the wave function (14), and taking into account the Wigner-Eckart theorem, we can present the angular matrix element as

$$\begin{aligned} \langle 12IM_I | A_{\Lambda} | 1'2'l'M_{l'} \rangle &= (-1)^{L_A + L_B + J_1 + J'_1 + J_2 + J'_2 + M_{F_1} + M_{F'_1} - \Omega'_1 - \Omega'_2 + M_{I-1}} \frac{[1 + \varepsilon_1 \varepsilon'_1 (-1)^{L_A}] [1 + \varepsilon_2 \varepsilon'_2 (-1)^{L_B}]}{2} \\ &\times ([I][I'] [J_1][J'_1][J_2][J'_2][F_1][F'_1][F_2][F'_2])^{1/2} \begin{pmatrix} L_A & L_B & L \\ M_{F_1} - M_{F'_1} & M_{F_2} - M_{F'_2} & M_I - M_{I'} \end{pmatrix} \\ &\times \begin{pmatrix} J'_1 & L_A & J_1 \\ \Omega'_1 & 0 & -\Omega_1 \end{pmatrix} \begin{pmatrix} J'_2 & L_B & J_2 \\ \Omega'_2 & 0 & -\Omega_2 \end{pmatrix} \begin{pmatrix} L_A & F_1 & F'_1 \\ M_{F_1} - M_{F'_1} & -M_{F_1} & M_{F'_1} \end{pmatrix} \\ &\times \begin{pmatrix} L_B & F_2 & F'_2 \\ M_{F_2} - M_{F'_2} & -M_{F_2} & M_{F'_2} \end{pmatrix} \begin{pmatrix} l' & L & l \\ M_{l'} & M_I - M_{I'} & -M_{I'} \end{pmatrix} \begin{pmatrix} l' & L & l \\ 0 & 0 & 0 \end{pmatrix} \\ &\times \begin{Bmatrix} L_A & F_1 & F_1 \\ I & J_1 & J_1 \end{Bmatrix} \begin{Bmatrix} L_B & F_2 & F_2 \\ I & J_2 & J_2 \end{Bmatrix}, \end{aligned} \quad (16)$$

where  $I = 1/2$  is each molecule's nuclear spin.

The matrix elements of the angular functions  $A_{\Lambda}$  between symmetrized basis states (15) are

$$\langle 12IM_I | A_{\Lambda}^s | 1'2'l'M_{l'} \rangle = \frac{\langle 12IM_I | A_{\Lambda}^s | 1'2'l'M_{l'} \rangle + (-1)^I \langle 21IM_I | A_{\Lambda}^s | 1'2'l'M_{l'} \rangle}{\sqrt{(1 + \delta_{1,2})(1 + \delta_{1',2'})}} \frac{1 + (-1)^{I+l'}}{2}. \quad (17)$$

In practice, before each scattering calculation we numerically transform the Hamiltonian matrix from this basis into the field-dressed basis defined by Eq. (7). The coupled-channel Schrödinger equations take the usual form

$$\left( \frac{d^2}{dR^2} \mathbf{I} + \frac{2m}{\hbar^2} [\mathbf{E} \mathbf{I} - \mathbf{E}_{th}(\mathcal{E}) - \mathbf{V}(R, \mathcal{E})] \right) \tilde{\psi}(R, \mathcal{E}) = 0, \quad (18)$$

where  $\mathcal{E}$  is the value of the electrostatic field and just a parameter for these equations,  $\mathbf{E}_{th}(\mathcal{E})$  is diagonal matrix of the threshold energies,

$$\begin{aligned} \mathbf{V}(R, \mathcal{E}) \Rightarrow & \{ \langle \tilde{1} | \otimes \langle \tilde{2} | \otimes \langle l M_l | \rangle \}^{s, \mathcal{M}} \\ & \times V(\omega_A, \omega_B, \omega, R) \{ | \tilde{1}' \rangle \otimes | \tilde{2}' \rangle \otimes | l' M_l' \rangle \}^{s, \mathcal{M}} \end{aligned} \quad (19)$$

is the matrix that contains the potential (10) and the centrifugal potential, and  $\tilde{\psi}(R, \mathcal{E})$  is the matrix of radial wave functions in the field-dressed basis:

$$\tilde{\Psi}^{\mathcal{M}} = \sum_{\tilde{1}, \tilde{2}, l, M_l} \{ | \tilde{1} \rangle \otimes | \tilde{2} \rangle \otimes | l M_l \rangle \}^{s, \mathcal{M}} \psi^{\mathcal{M}, \tilde{1}, \tilde{2}}(R, \mathcal{E}). \quad (20)$$

We solved these equations using a logarithmic derivative propagator method [24] to determine scattering matrices. As a rule the convergence to three digits was obtained by using three different integration steps: with 0.001 a.u. up to 100 a.u., then with 0.01 a.u. from 100 a.u. to 500 a.u., and then with 0.1 a.u. from 500 a.u. to 10 000 a.u. for collisional energies we used. It should be said that the choice of integration parameters depends on the value of electrostatic field too to get the given accuracy. Using these matrices, we calculate the total state-to-state cross sections and rate constants, according to the procedure described in Ref. [31].

#### IV. RESULTS

This paper considers the scattering problem for OH molecules in an electrostatic field for cold and ultracold temperatures. We are interested, in particular, in the highest-energy weak-field-seeking state of the ground rotational state,  $| (J, I) F M_F, \Omega \epsilon \rangle = | (3/2, 1/2) 22, 3/2, - \rangle$ . This state is indicated by the heavy solid line in Fig. 1. Since the quantum numbers  $J$ ,  $I$ , and  $\Omega$  are the same for all the scattering processes, we will refer to this state by the shorthand notation  $| F M_F, \epsilon \rangle = | 22, - \rangle$ .

The main novel feature of OH-OH scattering, as compared to atoms or nonpolar molecules, is the presence of the long-range dipole-dipole interaction and its dependence on the electrostatic field. Because these interactions strongly mix different partial waves, it is essential that we include more than one value of  $l$ . However, in the interest of emphasizing the basic underlying physics, we have included only the  $s$  and  $d$  partial waves. The sample calculations show that higher partial waves change the results only slightly at the energies considered. In this case, given the initial state with  $M_{F1} = M_{F2} = 2$ , the only allowed values of the total projection are  $\mathcal{M} = 2, 3, 4, 5, 6$ . Among these channels only the one with  $\mathcal{M} = 4$  contains a contribution from  $s$ -wave scattering, and so will deserve special attention in what follows. In this case, the total number of scattering channels for all allowed values of  $\mathcal{M}$  is 208.

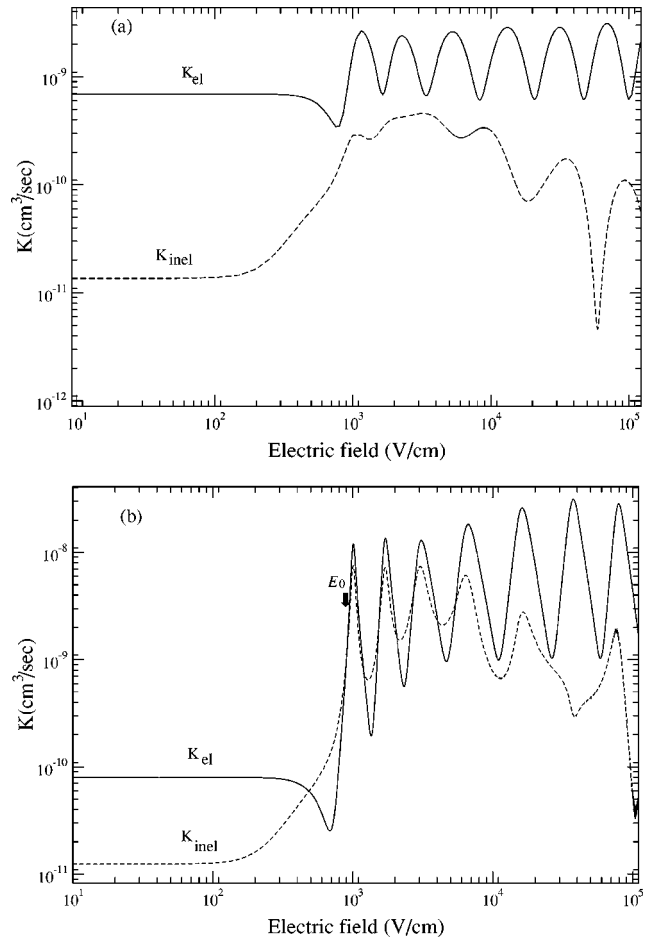


FIG. 2. Rate constants versus electric field for OH-OH collisions with molecules initially in their  $| F M_F, \epsilon \rangle = | 22, - \rangle$  state. Shown are the collision energies 100  $\mu\text{K}$  (a) and 1  $\mu\text{K}$  (b). Solid lines denote elastic-scattering rates, while dashed lines denote rates for inelastic collisions, in which one or both molecules change their internal state. These rate constants exhibit characteristic oscillations in field when the field exceeds a critical field  $\mathcal{E}_0 \approx 1000$  V/cm.

#### A. Prospects for evaporative cooling

One of the goals of the present work is to revisit the conclusions of Ref. [13], concerning the effectiveness of evaporative cooling for electrostatically trapped molecules. To this end Fig. 2 plots the elastic and state-changing inelastic rate constants versus field strength for two different collision energies, 100  $\mu\text{K}$  and 1  $\mu\text{K}$ . Here “elastic” refers to the collisions that do not change the internal state of either molecule, while “inel” denotes those collisions in which one or both molecules are converted into any other states. These transitions are typically exothermic, leading to trap heating. Not all of these collisions produce untrapped states, however. We find that the main contributions to the  $K_{inel}$  are given by processes in which quantum numbers  $F$  and/or  $M_F$  are changed by one. In particular, the process  $| 22, - \rangle + | 22, - \rangle \rightarrow | 22, - \rangle + | 21, - \rangle$  generally makes the largest contribution to  $K_{inel}$ , especially at high electric field.

At low field the rates are nearly independent of field, but begin to evolve when the field approximately exceeds the critical field  $\mathcal{E}_0 = \Delta/2\mu$ , where the Stark effect changes from

quadratic to linear. Above this field the rate constants exhibit oscillations as a function of the field. These oscillations provide an experimentally variable signature of resonant collisions, meaning that mapping this field dependence should help in untangling the details of the long-range OH-OH interaction. This is similar to the ability of the magnetic-field Feshbach resonances in the alkali atoms to yield detailed scattering parameters [29,30].

Following the example of ultracold atoms, we expect that evaporative cooling can proceed when the ratio of elastic to inelastic collisions  $K_{el}/K_{inel} \gg 1$ . Fig. 2 shows that this is hardly ever the case for large field values  $\mathcal{E} > \mathcal{E}_0$ , except, perhaps, at very special field values where  $K_{inel}$  is at a minimum of its oscillation. Since the losses are dominated by exothermic processes, the ratio  $K_{el}/K_{inel}$  in the threshold scattering limit scales as the ratio  $k_i/k_f$  of the incident and final channel wave numbers, as can be seen from the Born approximation. Thus at high electric fields, where the Stark splitting is large (hence  $k_f$  is large), the ratio may become more favorable. In our calculations, this apparently happens for fields above  $10^4$  V/cm.

For fields below  $\mathcal{E}_0 \approx 1000$  V/cm, a favorable ratio of  $K_{el}/K_{inel}$  is only somewhat more likely. For fields this low, however, the maximum depth of an electrostatic trap is  $\approx 8$  mK, as given by the magnitude of the Stark shift (Fig. 1). The temperature of the trapped gas must therefore be well below this temperature. In the example of a  $100\text{-}\mu\text{K}$  gas [Fig. 2(a)], the ratio  $K_{el}/K_{inel}$  may indeed be favorable. However, if the gas is cooled further, say to  $1\text{ }\mu\text{K}$  [Fig. 2(b)], this ratio becomes less favorable again. This is because of the Wigner threshold laws: the exothermic rate  $K_{inel}$  is energy independent at low energy, while the elastic scattering rate plummets to zero as the square root of collision energy. Thus, in general, evaporative cooling seems to be viable only over an extremely limited range of temperature and field for the OH molecule, if at all. We therefore reiterate the message of Ref. [13], and recommend that cold OH molecules be trapped by a far-off-resonance optical dipole trap in their lowest-energy  $|F| M_F, \epsilon\rangle = |11, +\rangle$  states.

At this point, we emphasize an essential difference between the evaporative cooling of electrostatically trapped polar molecules and of magnetically trapped paramagnetic molecules. For polar molecules, the transition from weak-to-strong field seeking states is *always* exothermic, even in zero applied field. This is because the lower member of a  $\Lambda$  doublet is always strong-field seeking (e.g., Fig. 1). For paramagnetic molecules, by contrast, weak- and strong-field seeking states can be nearly degenerate at low magnetic-field values (e.g.,  $^{17}\text{O}_2$  as discussed in Refs. [31,32]). In the present case, OH is also paramagnetic and hence could, in principle, be magnetically trapped. For example, the low-energy states with  $|F M_F, \epsilon\rangle = |11, +\rangle$  might be suitable candidates. The influence of electric dipole interactions on evaporative cooling of magnetically trapped OH has yet to be explored.

### B. Analysis of the long-range interaction

The general behavior of the rate constants in Fig. 2 can be explained qualitatively by simplifying our model even fur-

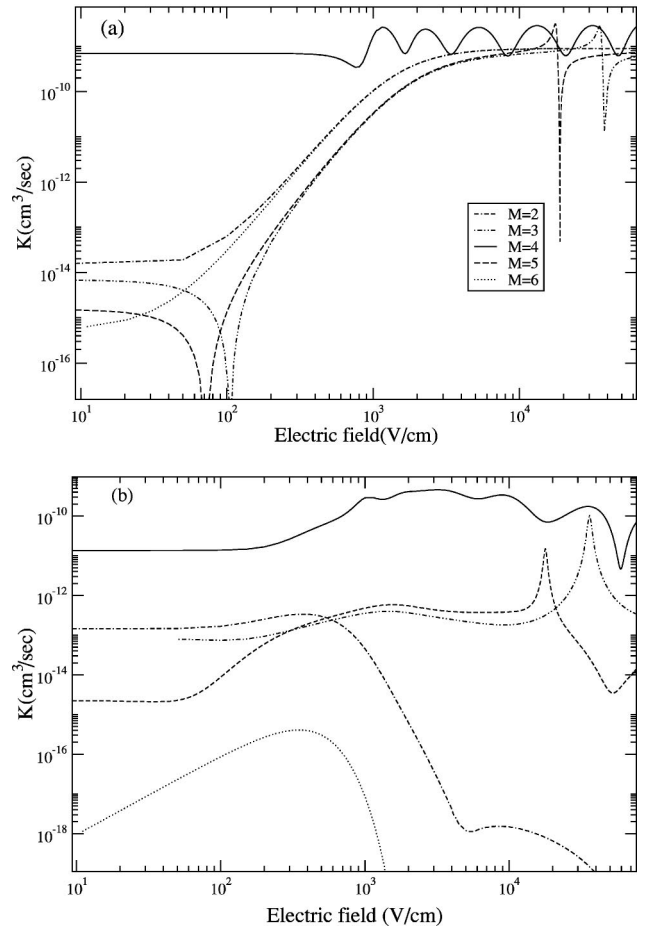


FIG. 3. Elastic (a) and inelastic (b) rate constants versus electric field for the same circumstances as in Fig. 2(a). The rates are separated into contributions from different values of  $\mathcal{M}$ , the projection of total angular momentum on the laboratory  $z$  axis.

ther to a case that contains only the essential ingredients: the dipole-dipole interaction, the  $\Lambda$  doublet, and an electric field [13]. Roughly speaking, the electric field has two effects on the molecules: (1) it mixes molecular states of opposite parity, thus creating induced dipole moments; and (2) the resulting dipole-dipole interaction strongly couples scattering channels with different partial waves, leading to long-range couplings between the two molecules.

As a starting point in this analysis, Figure 3 breaks down the elastic and inelastic rates into their contributions from different values of the total projection of angular momentum  $\mathcal{M}$ . This is done for the rates calculated at an energy  $E = 100\text{ }\mu\text{K}$ , from Fig. 2(a). In both elastic and inelastic scattering, the rates are dominated by the contribution from  $\mathcal{M} = 4$ , which, it will be recalled, is the only value of  $\mathcal{M}$  that incorporates  $s$  partial waves in the present model. We will accordingly consider only this case in what follows.

The model used to obtain the results in Figs. 2 and 3 consists of 32 channels for the block of the Hamiltonian matrix with  $\mathcal{M} = 4$ . To simplify the analysis of this block even further, we focus on the sub-Hamiltonian with fixed quantum numbers  $F = M_F = 2$  for each molecule. This reduces the effective Hamiltonian to six channels: there are

three nondegenerate thresholds  $E_{\varepsilon_1\varepsilon_2}$  corresponding to different possible values of the field-dressed parity quantum number  $\varepsilon_i = \pm$ . For each of these three thresholds there are two channels, corresponding at large  $R$  to  $s$  and  $d$  partial waves.

The simplified six-channel Hamiltonian matrix then consists of  $3 \times 3$  blocks  $\hat{V}^{ll'}$  parametrized by partial wave quantum numbers  $l, l'$ :

$$\hat{H} = \begin{pmatrix} \hat{V}_{diag}^{00} & \hat{V}_{\varepsilon}^{02} \\ \hat{V}_{\varepsilon}^{20} & \hat{V}_{diag}^{22} + \hat{V}_{\varepsilon}^{22} \end{pmatrix}. \quad (21)$$

Here the diagonal components  $\hat{V}_{diag}^{ll'}$  include the parity thresholds and the centrifugal interactions,

$$\hat{V}_{diag}^{ll} = \begin{pmatrix} E_{--} + \frac{\hbar^2 l(l+1)}{2mR^2} & 0 & 0 \\ 0 & E_{-+} + \frac{\hbar^2 l(l+1)}{2mR^2} & 0 \\ 0 & 0 & E_{++} + \frac{\hbar^2 l(l+1)}{2mR^2} \end{pmatrix}, \quad (22)$$

where the electric-field-dependent thresholds are given by  $E_{\varepsilon_1\varepsilon_2} = E_+ + E_- - (\varepsilon_1 + \varepsilon_2)\Delta\sqrt{1+k^2}/2$ , in terms of the dimensionless parameter

$$k \equiv \frac{2\langle 22, + | \vec{\mu} \cdot \vec{\mathcal{E}} | 22, - \rangle}{\Delta} \quad (23)$$

that relates the electric-field strength  $\mathcal{E}$  to the zero-field  $\Lambda$ -doublet splitting  $\Delta = E_- - E_+$ . The simplified field-dependent dipole-dipole interaction term  $\hat{V}_{\varepsilon}^{ll'}$  is readily parametrized in the field-dressed basis as

$$\hat{V}_{\varepsilon}^{ll'} = \begin{pmatrix} k^2 & -\sqrt{2}k & 1 \\ -\sqrt{2}k & 1-k^2 & \sqrt{2}k \\ 1 & \sqrt{2}k & k^2 \end{pmatrix} \frac{C^{ll'}}{(1+k^2)R^3}, \quad (24)$$

whose coefficient  $C^{ll'}$ , which is independent of both  $R$  and the electric field, is given by

$$C^{ll'} = -\mu^2 ([l][l'])^{1/2} \begin{pmatrix} l' & 2 & l \\ 0 & 0 & 0 \end{pmatrix}^2 \times \frac{\Omega^2 M_F^2 [J(J+1) + F(F+1) - I(I+1)]^2}{2[J(J+1)F(F+1)]^2}. \quad (25)$$

Notice that the dipole-dipole interaction vanishes for  $s$  waves, so that  $\hat{V}_{\varepsilon}^{00} = 0$ .

Within this simplified model, we will refer to the scattering channels by the parities  $\varepsilon_1$  and  $\varepsilon_2$  of the two molecules, along with the partial-wave quantum number  $l$ . Thus the incident channel for weak-field seekers will be denoted  $|\varepsilon_1\varepsilon_2, l\rangle = |--, 0\rangle$ . Recall that all other quantum numbers ( $J, I, \Omega, F, M_F$ ) are assumed to have fixed values for each molecule.

The explicit field dependence in the coupling matrix (24) explains qualitatively the behavior of our ultracold weak-field-seeking molecules which have incident quantum number  $\varepsilon = -$ . For zero electric field ( $k=0$ ), there is no direct dipole-dipole coupling between identical molecules. There is, however, an off-diagonal coupling to different channels with opposite parity, as can be seen in the form of the Hamiltonian (21). This interaction brings in the dipole-dipole coupling in second order, contributing an effective dispersion-like potential  $C_6^{eff}/R^6$ , with a coefficient

$$C_6^{eff} = \frac{(C^{20})^2}{2\Delta} \propto \frac{\mu^4}{\Delta}, \quad (26)$$

for both  $s$  and  $d$  partial waves. For the OH molecule this effective coefficient is  $\approx 4 \times 10^4$  a.u., far larger than for the alkali atoms that are familiarly trapped. Thus, even in zero external field the effective interaction strength of polar molecules is quite large. This may imply the breakdown of the contact-potential approximation in describing the Bose-Einstein condensates of polar molecules, even when their dipoles are not aligned by an external field [1–3]. We note that the quadrupole-quadrupole interaction is relatively unimportant, becoming larger than this effective dispersion interaction only when  $R > \approx 3 \times 10^5$  a.u.

When the field is switched on, the  $s$ -wave channels undergo a qualitative change. Now the incident channel  $|--, 0\rangle$  sees a direct coupling to its  $d$ -wave counterpart  $|--, 2\rangle$ , via the matrix element  $V^{l=0, l'=2} \propto [k^2/(1+k^2)] (\mu^2/R^3)$ . This perturbation generates an far stronger effective long-range potential of the form  $C_4^{eff}/R^4$ , with

$$C_4^{eff} = - \left( \frac{k^2}{1+k^2} \right)^2 \frac{\mu^4 2m}{l(l+1)}, \quad (27)$$

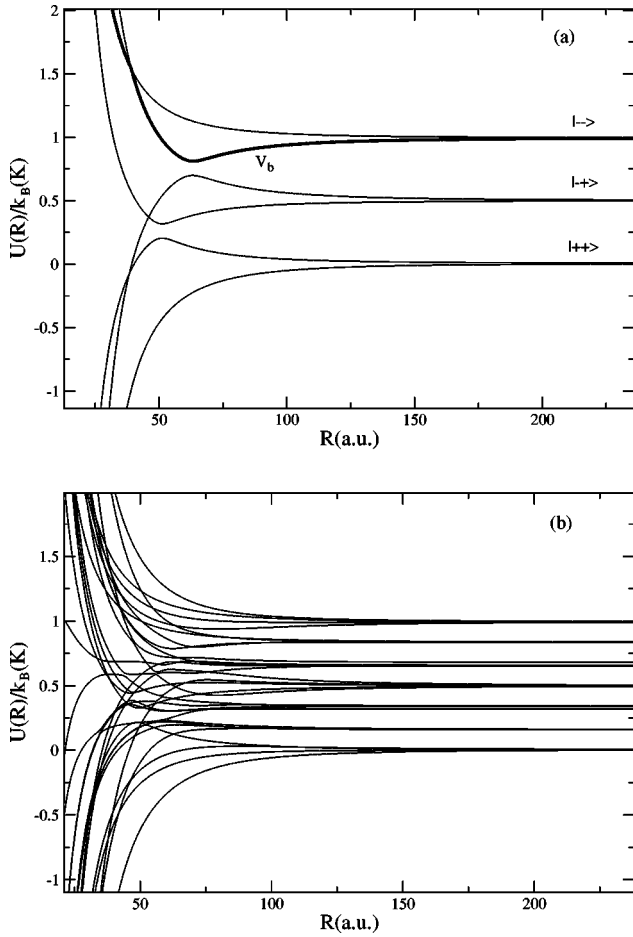


FIG. 4. Adiabatic potential-energy curves. The curves in (a) correspond to the simplified six-channel model described in the text, and show a long-range potential well (labeled  $V_b$ ) that can hold bound states of the  $[\text{OH}]_2$  dimer. The curves in (b) are those for the more complete calculation that includes hyperfine structure.

where  $l=2$ . Thus the electric field is able to completely alter the character of the intermolecular interaction.

For  $d$ -wave collisions, the dipole-dipole coupling is direct, but not in the limit of zero field where the molecules are in parity eigenstates. At low fields ( $k \ll 1$ , where the Stark effect is quadratic), the diagonal coupling  $V_{\mathcal{E}}^{22} \propto k^2/(1+k^2)$  is small. In this limit, the molecules are nearly in parity eigenstates, hence do not “know” that they have dipole moments. At larger fields this interaction grows in scale, thus “activating” the dipoles. This is why the rate constants shown in Figs. 2 and 3 begin to evolve at fields near  $\mathcal{E}=\mathcal{E}_0$ . It is also why the contributions from all the angular-momentum projections except the one with  $\mathcal{M}=0$  contribute only weakly to scattering at low field. The channels with  $\mathcal{M} \neq 4$  are all of  $d$ -wave character, hence obey a threshold law  $\sigma \propto E^2$  at low fields, then evolve to a  $\sigma \propto \text{const}$  threshold law at larger fields.

### C. Large-field oscillations and long-range states of the $[\text{OH}]_2$ dimer

At fields larger than the critical field  $\mathcal{E}_0$ , the rate constants in Fig. 2 exhibit oscillations with the field. Significantly,

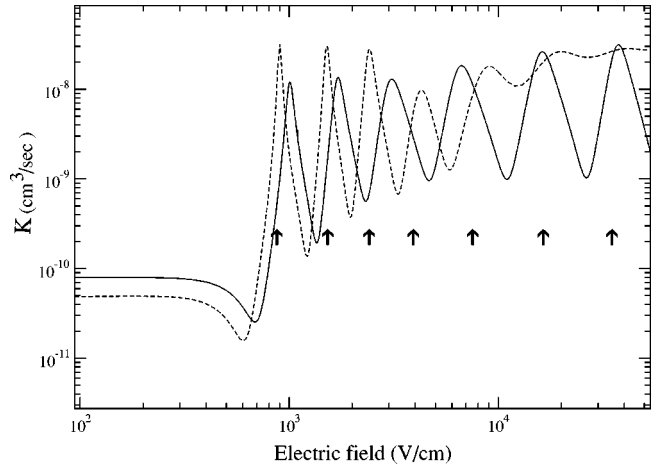


FIG. 5. Elastic rate constants versus field, as in Fig. 2. The solid line reproduces the elastic rate constant from Fig. 2. The dashed line is an approximate elastic rate constant based on the simplified six-channel model described in the text. The arrows indicate values of the electric field at which bound states of the long-range potential  $V_b$  (Fig. 4) coincide with the scattering threshold.

these occur only when the projection of the total angular momentum  $\mathcal{M}=4$ , which is the only case in which  $s$  and  $d$  partial waves are mixed (Fig. 3). To understand this oscillating behavior of cross sections, we show in Fig. 4(a) the adiabatic potential curves in the simplified six-channel model (21). In the case shown the field is  $\mathcal{E}=10^4$  V/cm. In this figure, a strong avoided crossing can be seen at  $R \approx 60$  a.u., corresponding to the crossing of the attractive  $| \varepsilon_1 \varepsilon_2, l \rangle = | - -, 0 \rangle$  channel with the repulsive  $| - +, 2 \rangle$  channel. The strong dipole-dipole interaction between these different partial waves creates the adiabatic potential shown as a heavy black line and labeled  $V_b$ .

This potential curve supports bound states of the  $[\text{OH}]_2$  dimer. These bound states are of purely long-range character, similar to the long-range states of the alkali dimers [33] which have been used in the in photoassociation spectroscopic studies of ultracold collisions [34,35]. Moreover, in the case of the  $[\text{OH}]_2$  states the shape of the potential  $V_b$ , hence the energies of the bound states, are strongly subject to the strength of the applied electric field. The curve in Fig. 4(a) in fact possesses no bound states in zero field, but five by the time the field reaches  $10^4$  V/cm. More realistic adiabatic potentials are, of course, more elaborate, as shown in Fig. 4(b) for the more complete Hamiltonian that includes hyperfine levels. Nevertheless, in this figure, too, can be seen adiabatic potential wells that will support bound states.

The significance of these curves is twofold: the crossing is very adiabatic, implying that coupling to lower-energy channels is weak, and that therefore the cross sections depend only weakly on details of the short-range potentials. This we have indeed verified by altering the short-range potential in the full calculation.

Additionally, as the field strength grows and the potential becomes deeper, new bound states are added to the potential, causing scattering resonances to appear. This is the cause of the oscillations observed in the rate constants in Fig. 2. To

illustrate this, we reproduce in Fig. 5 the complete elastic-scattering rate constant (solid line), along with the same quantity as computed in the simple six-channel model (dashed line). The qualitative behavior is nearly the same, namely, oscillations appear at fields above  $\mathcal{E}_0$ . Moreover, the arrows in the figure indicate the values of the field for which a bound state of  $V_b$  coincides with the scattering threshold. These fields correspond fairly well to the peaks, although they are somewhat offset by coupling to other channels. Nevertheless, this simple picture clearly identifies the origin of these oscillations with the existence of long-range bound states.

These resonant states are not Feshbach resonances, since there is no excitation of internal states of the molecules; nor are they shape resonances in the usual sense, since there is no barrier through which the wave function must tunnel. Instead, they are the direct result of altering the interaction potential to place a bound state exactly at threshold [14]. Probing these states through direct scattering of weak-field-seeking states should reveal details about the long-range OH-OH interaction, making possible a comparison of theory and experiment without the need to fully understand the short-range  $[\text{OH}]_2$  potential-energy surface.

## V. CONCLUSION

In this paper, we theoretically investigated ultracold collisions of ground-state polar diatomic molecules in an electrostatic field, taking OH molecules as a prototype. Focusing on weak-field-seeking states, we have strengthened the suppositions in Ref. [13] that the long-range dipolar interactions

drive inelastic-scattering processes that are generally unfavorable for evaporative cooling of this species. However, at electric fields above a characteristic value  $\mathcal{E}_0$ , oscillations occur in both elastic and inelastic collision rates, implying that a regime may be found where the ratio  $K_{elastic}/K_{inel}$  is favorable for cooling. Even though evaporative cooling may be difficult, the inelastic rates may nevertheless prove useful diagnostic tools for cold collisions of these molecules. The Stark slowing technique provides a means of launching a bunch of molecules toward a stationary trapped target, i.e., of making a real scattering experiment [12,17].

For actual trapping and cooling purposes, for instance as a means of producing molecular Bose-Einstein condensates or degenerate Fermi gases, it seems likely that the molecules must be trapped in their strong-field-seeking states. Collisions of these species will present their own difficulties, since they will depend strongly on the short-range part of the potential-energy surface. However, the scattering length for OH-OH scattering may be determined by photoassociation spectroscopy to the long-range bound states we have described above. This will be analogous to the determination of alkali scattering lengths [34,35], except that microwave, rather than optical, photons will be used. The detailed properties of the long-range  $[\text{OH}]_2$  states, and prospects for using them in this way, therefore deserve further attention.

## ACKNOWLEDGMENTS

This work was supported by the National Science Foundation. We acknowledge useful discussions with J. Hutson and G. Shlyapnikov.

- 
- [1] L. Santos, G.V. Shlyapnikov, P. Zoller, and M. Lewenstein, *Phys. Rev. Lett.* **85**, 1791 (2000); Stefano Giovanazzi *et al.*, *J. Phys. B* **34**, 4757 (2001).
- [2] S. Yi and L. You, *Phys. Rev. A* **63**, 053607 (2001).
- [3] K. Góral, K. Rzążewski, and T. Pfau, *Phys. Rev. A* **61**, 051601 (2000); J.-P. Martikainen, M. Mackie, and K.-A. Suominen, *ibid.* **64**, 037601 (2001).
- [4] M.A. Baranov, M.S. Mar'enko, V.S. Rychkov, and G.V. Shlyapnikov, *Phys. Rev. A* **66**, 013606 (2002).
- [5] D. DeMille, *Phys. Rev. Lett.* **88**, 067901 (2002).
- [6] J.P. Shaffer, W. Chalupczak, and N.P. Bigelow, *Phys. Rev. Lett.* **82**, 1124 (1999).
- [7] U. Schlöder, C. Silber, and Z. Zimmerman, *Appl. Phys. B: Lasers Opt.* **73**, 801 (2001).
- [8] J.D. Weinstein, R. deCarvalho, T. Guillet, B. Friedrich, and J.M. Doyle, *Nature (London)* **395**, 148 (1998).
- [9] D. Egorov, J.D. Weinstein, D. Patterson, B. Friedrich, and J.M. Doyle, *Phys. Rev. A* **63**, 030501 (2001).
- [10] H.L. Bethlem, G. Berden, A.J. van Roij, F.M.H. Crompvoets, and G. Meijer, *Phys. Rev. Lett.* **84**, 5744 (2000).
- [11] H.L. Bethlem, G. Berden, F.M.H. Crompvoets, R.T. Jongma, A.J.A. van Roij, and G. Meijer, *Nature (London)* **406**, 491 (2000).
- [12] H. L. Bethlem, F. M. H. Crompvoets, R. T. Jongma, S. Y. T. van der Meerakker, and G. Meijer, *Phys. Rev. A* **65**, 053416 (2002).
- [13] John L. Bohn, *Phys. Rev. A* **63**, 052714 (2001).
- [14] L. D. Landau and E. M. Lifshitz, *Quantum Mechanics: Non-Relativistic Theory*, 4th ed. (Nauka, Moscow, 1989).
- [15] R. Shakeshaft, *J. Phys. B* **5**, L115 (1972).
- [16] B. Deb and L. You, *Phys. Rev. A* **64**, 022717 (2001).
- [17] J. Ye (private communication).
- [18] J.A. Coxon, *Can. J. Phys.* **58**, 933 (1980); Thomas D. Varberg and Kenneth M. Evenson, *J. Mol. Spectrosc.* **157**, 55 (1993).
- [19] Bernd Kuhn *et al.*, *J. Chem. Phys.* **111**, 2565 (1998).
- [20] Lawrence B. Harding, *J. Phys. Chem.* **95**, 8653 (1991).
- [21] A.G. Wickham and D.C. Clary, *J. Phys. Chem.* **98**, 420 (1992).
- [22] A.I. Maergoiz, E.E. Nikitin, J. Troe, and V.G. Ushakov, *J. Chem. Phys.* **105**, 6277 (1996).
- [23] N. Balakrishnan and A. Dalgarno, *Chem. Phys. Lett.* **341**, 652 (2001).
- [24] B.R. Johnson, *J. Comput. Phys.* **13**, 445 (1973).
- [25] M. Mizushima, *The Theory of Rotating Diatomic Molecules* (Wiley, New York, 1975); Helene Lefebvre-Brion, and Robert W. Field, *Perturbations in the Spectra of Diatomic Molecules* (Academic Press, London, 1986); Karl F. Freed, *J. Chem. Phys.* **45**, 4214 (1966).
- [26] Steven M. Miller and David C. Clary, *J. Chem. Phys.* **98**, 1843 (1993).

- [27] K. Schreel and J.J. Meulen, *J. Phys. Chem. A* **101**, 7639 (1997).
- [28] Ad van der Avoird, *Top. Curr. Chem.* **93**, 1 (1980).
- [29] J.L. Roberts, J.P. Burke, S.L. Cornish, N.R. Claussen, E.A. Donley, and C.E. Wieman, *Phys. Rev. A* **64**, 024702 (2001).
- [30] T. Loftus, C. A. Regal, C. Ticknor, J. L. Bohn, and D. S. Jin, *Phys. Rev. Lett.* **88**, 173201 (2002).
- [31] Alexandr V. Avdeenkov and John L. Bohn, *Phys. Rev. A* **64**, 052703 (2001).
- [32] A. Volpi and J.L. Bohn, *Phys. Rev. A* **65**, 052712 (2002).
- [33] M. Movre and G. Pichler, *J. Phys. B* **10**, 2631 (1977); W.C. Stwalley, Y.-H. Uang, and G. Pichler, *Phys. Rev. Lett.* **41**, 1164 (1978).
- [34] K.M. Jones, P.S. Julienne, P.D. Lett, W.D. Phillips, E. Tiesinga, and C.J. Williams, *Europhys. Lett.* **35**, 85 (1996).
- [35] J.P. Burke, Jr., *et al.*, *Phys. Rev. A* **60**, 4417 (1999); C.J. Williams *et al.*, *ibid.* **60**, 4427 (1999).